Dalton Transactions

ROYAL SOCIETY OF CHEMISTRY

PAPER

View Article Online
View Journal | View Issue

Cite this: *Dalton Trans.*, 2025, **54**, 9770

Relationship between molecular structures and thermogravimetric properties of gallium–amidinate based compounds†

Paul-Alexis Pavard,[a] Eva Pugliese,[a,b] Damien Coutancier,[a] Valérie Albin,[c] Nicolas Casaretto,[b] Sophie Bourcier,[b] Virginie Lair,[c] Armelle Ringuede,[c] Audrey Auffrant[b] and Nathanaelle Schneider*[a]

The ability to predict the thermal properties of molecular compounds is essential for their successful integration into vapor-phase processes such as atomic layer deposition (ALD) and chemical vapor deposition (CVD), as well as in catalysis and materials synthesis. In this work, we present a systematic study of 24 gallium amidinate complexes, designed to explore the relationship between molecular structure and thermal behavior. The series encompasses a range of structural variations: different ligand substituents, molecular symmetry, and co-ligands. Structural characterization, including in some cases single-crystal X-ray diffraction, was combined with detailed thermal analysis using thermogravimetric analysis (TGA) and differential scanning calorimetry (DSC) under both atmospheric and reduced pressure conditions. The results reveal clear correlations between thermal properties and ligand architecture, with features such as alkyl chain type, methyl group presence, and overall symmetry playing key roles in determining volatility and stability. Importantly, both symmetric and dissymmetric complexes were found to possess the desired thermal characteristics for vapor-phase deposition processes. Beyond offering valuable design principles for gallium precursors, the dataset generated herein provides a foundation for improving predictive models—empirical and AI-driven alike—towards the rational development of next-generation functional molecular compounds.

Received 22nd April 2025,
Accepted 26th May 2025

DOI: 10.1039/d5dt00944h

rsc.li/dalton

Introduction

Thermal properties of molecular compounds play a crucial role in a wide range of applications, including materials synthesis *via* atomic layer deposition (ALD) or chemical vapour deposition (CVD),[1] energy storage,[2] environmental applications,[3–6] catalysis,[7–12] chemical formulation,[13] and the determination of their shelf life.[14–16] Indeed, in the context of materials chemistry, these properties are particularly important when designing functional molecules, especially as precursors for vapour-phase processes. A thorough understanding of thermal behaviour is also essential for evaluating molecular stability under operational conditions, ensuring reliable performance in targeted applications.

Based on this, predicting the thermal properties of molecular compounds is very important and remains a critical challenge. Empirical approaches, based on established structure–property relationships and chemical intuition, have historically guided the development of predictive rules.[17–22] More recently, the emergence of artificial intelligence (AI) and machine learning has opened new avenues for forecasting thermal behaviour, offering data-driven models capable of identifying complex, non-linear patterns across diverse chemical families.[23–26] Quantitative structure–property relationship (QSPR)[27–30] or group-contribution (GC)[31–34] approaches being empirical models, they inherently lack predictive accuracy for entirely novel materials that significantly differ from the compounds in the training dataset.[35] In all cases, predictions must be anchored in experimental validation—either to confirm model accuracy or to generate robust datasets for further algorithm training and refinement.

To explore the relationship between molecular structure and thermal behaviour and evaluate the validity of empirical structure–property correlations across different structural

[a]*Institut Photovoltaïque d'Île-de-France (IPVF), UMR 9006, CNRS, Ecole Polytechnique - IP Paris, Chimie Paristech - PSL, 18 Boulevard Thomas Gobert, Palaiseau, 91120, France. E-mail: nathanaelle.schneider@cnrs.fr*
[b]*Laboratoire de Chimie Moléculaire (LCM), CNRS, école Polytechnique, Institut Polytechnique de Paris, Route de Saclay, 91120 Palaiseau, France*
[c]*PSL University, Chimie ParisTech, CNRS, Institut de Recherche Chimie Paris (IRCP), 11, rue Pierre et Marie Curie, F-75231 Paris, France*

† Electronic supplementary information (ESI) available. CCDC 2444176–2444185. For ESI and crystallographic data in CIF or other electronic format see DOI: https://doi.org/10.1039/d5dt00944h

motifs, we designed a systematic study involving a large set of molecular species. We selected gallium as metal centre and amidinate-based molecules as ligands,[36–40] due to the specific interest in this class of compounds to generate gallium-based thin films.[41,42] These include gallium complexes with one or two amidinate ligands, featuring various substituents in a symmetric or dissymmetric arrangement, and chloride or methyl as additional ligand. Whenever possible, advanced structural characterization was performed, including single-crystal X-ray diffraction, to provide unambiguous insight into molecular geometry and intermolecular interactions. Thermal properties were assessed both through direct thermal analysis—using thermogravimetric analysis (TGA) and differential scanning calorimetry (DSC) under atmospheric and reduced pressure—and indirectly through their behaviour during purification *via* distillation or sublimation. These combined data offer a robust basis to examine how specific structural features govern volatility and thermal stability.

Results

Synthesis of molecular species

Inspired by the work of Dagorne *et al.*[43] and Coles *et al.*,[44] a modular synthesis protocol was established to generate a library of gallium amidinate complexes differing in their molecular mass, steric hindrance and symmetry. Scheme 1 depicts the reaction scheme of the synthesis routes to obtain gallium amidinate complexes. Different commercially available organolithium compounds (R^3Li) were used during the synthesis of lithium amidinate complexes (1st step), allowing to vary the steric effects induced by the substituents. One equivalent of carbodiimide (R^1–N=C=N–R^2) was reacted with one equivalent of the organolithium in diethyl ether at 0 °C and the resulting solid was washed with pentane and characterised by NMR spectroscopy and X-ray crystallography when possible. Nine lithium amidinate complexes were synthesised, with average to good yields (Y = 49 to 93%). To obtain the gallium complexes, the lithium amidinates were reacted with gallium trichloride in a transmetallation reaction. The mono ($(\mathbf{L}^n)\mathbf{GaCl_2}$) and bis-amidinate ($(\mathbf{L}^n)_2\mathbf{GaCl}$) complexes were both obtained by controlling the stoichiometry between the lithium amidinate and the gallium salt. The complexes were purified either by sublimation (for solids) or by vacuum distillation (for oils). For this step, the yields obtained varied noticeably (Y = 29 to 90%). Bis-amidinate gallium complexes could not be obtained from the $\mathbf{L^4Li}$, $\mathbf{L^5Li}$, $\mathbf{L^7Li}$ and $\mathbf{L^9Li}$ complexes, even upon heating as confirmed by the persistence of the lithium amidinate signals in the ^{1}H-NMR spectra. This is most likely due to steric effects induced by the bulky ligands that restricts the coordination to one ligand.[45–49] Lastly, the gallium methyl complexes were prepared by reaction of $(\mathbf{L}^n)_x\mathbf{GaCl_{3-x}}$ with x equivalents of methyllithium (MeLi). The resulting $(\mathbf{L}^n)\mathbf{GaMe_2}$ and $(\mathbf{L}^n)_2\mathbf{GaMe}$ complexes were either in oil forms and were purified by vacuum distillation or in solid forms and purified by sublimation ($(\mathbf{L^1})\mathbf{GaMe_2}$, $(\mathbf{L^2})_2\mathbf{GaMe}$ and $(\mathbf{L^6})_2\mathbf{GaMe}$). The obtained yields varied over a large range (Y = 13 to 80%), however most of the chlorinated gallium amidinate complexes could be transformed into their methyl counterparts. Note that some of these complexes were previously reported.[41,43–45,50–52]

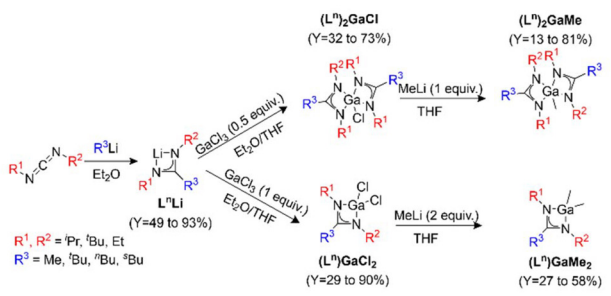

Scheme 1 General procedure for the synthesis of gallium amidinate complexes.

The individual yields for all the gallium complexes are reported in Table 1, together with the purification temperatures by sublimation or distillation, which were recorded under a static vacuum of the order of 5×10^{-2} mbar. These temperatures do not appear to depend solely on the molar mass of the complex. The difference between mono- and bis-amidinate is pronounced; the $(\mathbf{L}^n)\mathbf{GaCl_2}$ complexes have a vaporization temperature below 100 °C, unlike the $(\mathbf{L}^n)_2\mathbf{GaCl}$ complexes, which vaporise above 110 °C. The $(\mathbf{L^3})_2\mathbf{GaCl}$ complex, not being volatile enough, was purified by extraction. The steric hindrance of linear or branched alkyl chains is also an important parameter since $(\mathbf{L^1})\mathbf{GaCl_2}$ (with C^{t}Bu), $(\mathbf{L^3})\mathbf{GaCl_2}$ (with C^{n}Bu) and $(\mathbf{L^4})\mathbf{GaCl_2}$ (with C^{s}Bu), have sublimation temperatures of 100 °C, 80 °C and 80 °C respectively. Fig. 1 shows an overlay of the different ^{1}H-NMR spectra obtained for the complexes with the ($\mathbf{L^2}$) ligand. In this example, the ligand protons are characterised by three resonances a quadruplet, a doublet, and a singlet corresponding respectively to the CH and CH_3 of the isopropyl groups and that of the endocyclic methyl. It highlights how from one lithium amidinate complex, four gallium amidinate complexes could be synthesised by tuning the number of equivalents of the gallium salt, and how these complexes are easily distinguishable by ^{1}H-NMR analysis. In addition to the different chemical shifts in these five complexes, methyl groups bonded to the gallium led to a more shielded resonance (δ = −0.5–0.5 ppm). These chemical shifts are in agreement with literature precedents.[43] More details on all of the reaction steps and characterizations can be found in the ESI.†

Gallium amidinate complexes were crystallised when possible by sublimation or by slow evaporation of the pure product in a highly volatile solvent such as pentane. The crystal structures with the ($\mathbf{L^2}$) amidinate are shown in Table 2, as a representative example. The other structures and more details can be found in the ESI (Tables S1–S6†).

Crystals suitable for single-crystal X-ray diffraction are generally more readily obtained from chlorinated gallium com-

Table 1 Gallium amidinate complexes synthesised reported with their yield and the temperature of purification

		 $\mathbf{L^1Li}$	 $\mathbf{L^2Li}$	 $\mathbf{L^3Li}$	 $\mathbf{L^4Li}$	 $\mathbf{L^5Li}$	 $\mathbf{L^6Li}$	 $\mathbf{L^7Li}$	 $\mathbf{L^8Li}$	 $\mathbf{L^9Li}$
	$\mathbf{(L^n)GaCl_2}$	90% 100 °C[a]	55% 50 °C[a]	50% 80 °C[a]	82% 80 °C[a]	68% 100 °C[a]	68% 85 °C[a]	29% 50 °C[b]		63% 70 °C[a]
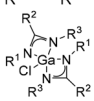	$\mathbf{(L^n)_2GaCl}$	37% 120 °C[a]	62% 115 °C[a]	62%	—	—	32% 150 °C[a]	—	—	—
	$\mathbf{(L^n)GaMe_2}$	34% 50 °C[a]	55% <25 °C[b]	29% 50 °C[b]	58% <25 °C[b]	41% 75 °C[b]	49% <25 °C[b]	30% 40 °C[b]	27% <25 °C[b]	50% <25 °C[b]
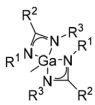	$\mathbf{(L^n)_2GaMe}$		54% 150 °C[a]	81%			13% 90 °C[a]			

[a] For sublimation under a dynamic vacuum of 5×10^{-2} mbar. [b] For distillation under a dynamic vacuum of 5×10^{-2} mbar.

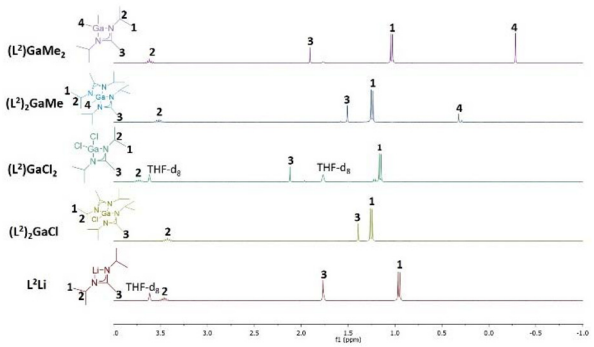

Fig. 1 Superposition of ^{1}H NMR spectra of $\mathbf{L^2Li}$, $\mathbf{(L^2)GaCl_2}$, $\mathbf{(L^2)_2GaCl}$, $\mathbf{(L^2)GaMe_2}$ and $\mathbf{(L^2)_2GaMe}$.

plexes than from their methylated counterparts. While the former typically form solids, the latter are often oily substances that can only be crystalized at low temperatures, as observed for the $\mathbf{(L^5)GaMe_2}$ complex.

Gallium complexes all crystallise as monomers with amidinate ligands coordinated in κ^2-coordination mode. The gallium metal centre is tetracoordinated in mono-amidinate complexes that exhibit a distorted tetrahedral geometry, or pentacoordinated in the case of bis-amidinate complexes. The parameter τ_5 is useful to determine the geometry of distorted pentacoordinated complexes giving a value of 0 for a regular square-based pyramidal geometry to and 1 for a regular trigonal bi-pyramidal (see τ_5 values in Table 2, and in ESI, Table S6†).[53,54] $\mathbf{(L^n)_2GaCl_2}$ complexes present a distorted trigonal bi-pyramidal geometry according to τ_5 value closer to 1 than to 0 in all the cases.

Table 2 Crystallographic structures obtained for the gallium amidinate complexes with the $\mathbf{(L^2)}$ amidinate. In the table, the bond lengths Ga–N/Ga–X (where X = Cl or Me) and N–C are reported (in Å), as well as the chelation angle (NCN) and the τ_5 parameter for penta-coordinated complexes

	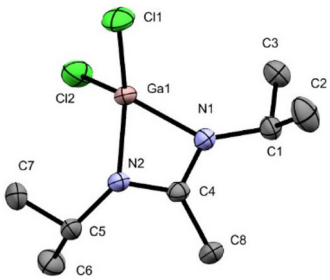	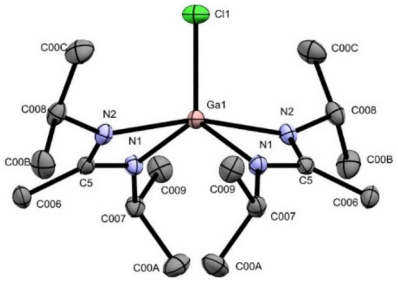	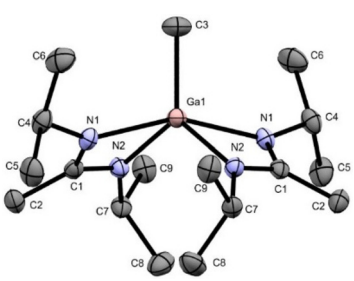
	$\mathbf{(L^2)GaCl_2}$	$\mathbf{(L^2)_2GaCl}$	$\mathbf{(L^2)_2GaMe}$
	$\widehat{\mathrm{NCN}} = 110.3(3)°$	$\widehat{\mathrm{NCN}} = 111.45(7)°$; $\tau_5 = 0.706$	$\widehat{\mathrm{NCN}} = 111.80(17)°$; $\tau_5 = 0.705$
Ga—X	2.1465(9); 2.1484(9)	2.2067(3)	1.960(3)
Ga—N	1.943(3); 1.943(2)	1.9578(7); 2.1306(6)	1.9590(17); 2.2156(16)
N—C	1.334(4); 1.321(4)	1.3440(10); 1.3211(10)	1.314(3); 1.346(2)

Based on its higher value for $(L^1)_2GaCl$ and $(L^6)_2GaCl$ complexes, their geometry is closer to a regular trigonal bipyramid that may be explained by the more important steric hindrance on the amidinate compared to the (L^2) ligand. The NCN angle of the amidinate ligand also depends on the steric effects, in particular that of the endocyclic alkyl substituent. In general, the larger the substituent, the smaller the angle. This trend is obvious when comparing the (L^5) and (L^1) complexes with those of (L^2) and (L^6). Substituting isopropyl with *tert*butyl groups at peripheral position seems to have a lower impact. Nevertheless, the NCN angle tends to decrease when increasing the bulkiness of the group (compare $(L^1)GaCl_2$ with $(L^5)GaCl_2$ and $(L^2)GaCl_2$ with $(L^6)GaCl_2$)[55] (see Table S-6).

Comparing the mono and bis-amidinate complexes, an elongation of the Ga—N bonds (average of 2.05 Å for bis- and of 1.94 Å for mono-ligated complexes) together with a reduction of the bite angles (65.4° on average for $(L^n)_2GaCl$ *vs.* 68.4° on average for $((L^n)GaCl_2)$) are observed. The N—C bond lengths of the amidinate ligand backbone are between 1.31 and 1.36 Å indicating a bond order of 1.5 for all the complexes and in agreement with previous reports.[43]

Thermal analysis of gallium–amidinate complexes

The synthesised gallium amidinate complexes were characterised by TG/DSC to assess their thermal properties. Each compound was analysed under atmospheric pressure (N_2) and reduced pressure (~1 mbar, N_2). Atmospheric pressure analyses facilitate comparison with literature data, as most thermal studies are conducted under inert or non-inert atmosphere at ambient pressure, while reduced-pressure analyses better simulate specific applications such as ALD/CVD precursor transport conditions. The TG/DSC temperature program follows a three-step process, detailed in the ESI (Fig. S2 and S3†), along with data processing steps. For each complex, the onset temperature of evaporation/sublimation (T_{onset}) and the residual mass percentages ($\%_{res}$) were extracted from the recorded curves and are summarised in Table 3.

The TG/DSC curves under both atmospheric and reduced pressure conditions are provided in the ESI (Fig. S4-1, S4-2 and S4-3†). $(L^n)_2GaCl$ complexes were excluded from TG/DSC analyses due to their low volatility, observed during the purification step.

Mass loss profiles varied depending on the analysis conditions (atmospheric *vs.* reduced pressure) and the type of amidinate complex. The 20 gallium amidinate complexes analysed exhibited distinct thermal profiles, with $\%_{res}$ values from −2% to 26%. As expected, TG/DSC analyses under reduced pressure generally resulted in lower residual percentages than those conducted at atmospheric pressure. Most complexes showed residual masses below 10%, except for $(L^6)_2GaMe$, $(L^2)_2GaMe$, and $(L^2)GaMe_2$.

DTG curves were particularly useful in identifying whether a complex vaporised as a single species or as multiple species. Reduced-pressure TG analyses generally led to a single-step vaporization for gallium amidinates, while atmospheric-pressure TG analyses of $(L^n)GaCl_2$ complexes mostly resulted in thermal decomposition, despite the formation of volatile products, as indicated by their low residual masses. Black residue observed in crucibles after analyses further confirmed decomposition under atmospheric pressure conditions. $(L^n)GaMe_2$ complexes demonstrated the most favourable behaviour across all conditions, with minimal decomposition. The only exception was $(L^2)GaMe_2$, which showed thermal degradation in the TG curve. The DSC curves of gallium amidinate complexes predominantly showed endothermic peaks: two for most solid complexes, a single peak for oil-like complexes. The endothermic peak attributed to the melting of solid complexes

Table 3 Thermal properties of selected compounds: onset vaporization temperatures (T_{onset}, in °C) and residual mass percentages ($\%_{res}$). Values in brackets correspond to analyses performed under reduced pressure

	$(L^n)GaCl_2$	$(L^n)GaMe_2$	$(L^n)_2GaMe$
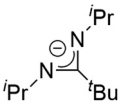 (L^1)	T_{onset} = 214 (117) $\%_{res}$ = 16 (4)	T_{onset} = 184 (60) $\%_{res}$ = 16 (11)	
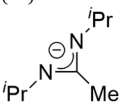 (L^2)	T_{onset} = 216 (91) $\%_{res}$ = 8 (−2)	T_{onset} = 129 (25) $\%_{res}$ = 12 (26)	T_{onset} = 218 (102) $\%_{res}$ = 10 (22)
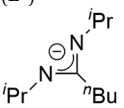 (L^3)	T_{onset} = 244 (100) $\%_{res}$ = 15 (10)	T_{onset} = 191 (75) $\%_{res}$ = 5 (3)	T_{onset} = 264 (126) $\%_{res}$ = 5 (10)
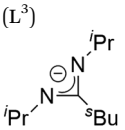 (L^4)	T_{onset} = 225 (94) $\%_{res}$ = 3 (6)	T_{onset} = 184 (58) $\%_{res}$ = 8 (7)	
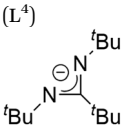 (L^5)	T_{onset} = 230 (128) $\%_{res}$ = 11 (1)	T_{onset} = 206 (91) $\%_{res}$ = 4 (2)	
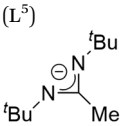 (L^6)	T_{onset} = 235 (109) $\%_{res}$ = 6 (4)	T_{onset} = 174 (47) $\%_{res}$ = 4 (7)	T_{onset} = 239 (125) $\%_{res}$ = 11 (15)
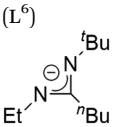 (L^7)	T_{onset} = 224 (85) $\%_{res}$ = 9 (4)	T_{onset} = 193 (71) $\%_{res}$ = 5 (5)	
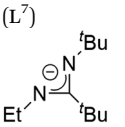 (L^8)		T_{onset} = 179 (67) $\%_{res}$ = 8 (2)	
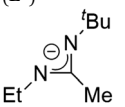 (L^9)	T_{onset} = 227 (89) $\%_{res}$ = 11 (6)	T_{onset} = 155 (35) $\%_{res}$ = 6 (10)	

remained unaffected by pressure, as these compounds are low-compressibility materials, a behaviour also observed in cesium hafnium chloride.[56] Based on the onset vaporization temperatures at both atmospheric and reduced pressure, methylated complexes exhibited higher volatility than their chlorinated counterparts. The vaporization energies, evaluated by integrating the peak area, do not represent the absolute values for gallium amidinate compounds, as the platinum rod calibration was not performed using a set of commercial compounds under identical experimental conditions (see ESI, Fig. S5†). However, the relative values remain valid, as the energy values were normalised per mole of compound. Thus, reduced-pressure TG/DSC required less energy for vaporization compared to atmospheric pressure. **(L^n)GaCl$_2$** complexes exhibited high vaporization energies under atmospheric pressure, likely contributing to multi-species volatilization and black residue formation due to decomposition. **(L^n)GaMe$_2$** complexes had the lowest vaporization energies among the tested compounds, indicating higher volatility.

The combination of TG/DSC analyses under different pressures enabled the identification of sublimable solid complexes by comparing their DSC curves. For example, in reduced-pressure TG/DSC of **(L^1)GaCl$_2$**, the presence of a single endothermic peak suggests that the complex undergoes sublimation. However, in atmospheric pressure TG/DSC, two endothermic peaks appear in the DSC signal, indicating a different thermal behaviour.

Discussion

We have described the synthesis of a series of gallium amidinate complexes along with their structural and thermal characterization.

The purification vaporization temperatures (T_{purif}), *i.e.* the temperature of appearance of a solid on the sublimation finger or the first liquid droplets during distillation, are slightly lower but align with the onset vaporization temperatures (T_{onset}) determined by TG/DSC. This confirms that volatility estimates from purification are consistent with TG/DSC results. This diversity of ligand and complexes further enables a discussion on the relationship between structure and thermal properties.

The first widely accepted correlation is between vaporization temperature and molecular weight. This trend is confirmed here: the lighter complexes (**(L^n)GaMe$_2$**) are the most volatile, while the heavier ones (**(L^n)$_2$GaMe**) exhibit the lowest volatility in our series. However, as shown in Fig. 2, volatility is not solely determined by molecular weight. For example, **(L^3)GaMe$_2$**, **(L^5)GaMe$_2$** and **(L^8)GaMe$_2$** complexes are among the heaviest but also show very good volatility.

The symmetry of the molecular compound is also known to influence the thermal properties. To show it, we compare complexes with identical molecular weight and branching on the endocyclic carbon but different lateral substituents. Thus, **(L^3)**-based complexes feature two ^{i}Pr groups, while **(L^7)**-based complexes have ^{t}Bu and Et substituents, introducing dissymmetry into the complex. Although their onset vaporization temperatures are similar, **(L^7)** exhibits lower residual mass after TG/DSC ($\%_{res}$ < 10%), suggesting that the ligand dissymmetry may contribute to an enhanced volatility. Similar observations can be made on **(L^1)**/**(L^8)** and **(L^2)**/**(L^9)**-based complexes. Among all those, increased dissymmetry from lateral substituents appears to improve thermal properties, leading to higher volatility and lower residual mass in chlorinated complexes (see ESI, Fig. S6†). Branching also plays a significant role, as illustrated by the complexes bearing **(L^1)**, **(L^3)**, and **(L^4)** ligands, which have the same molecular weight but differ in the substi-

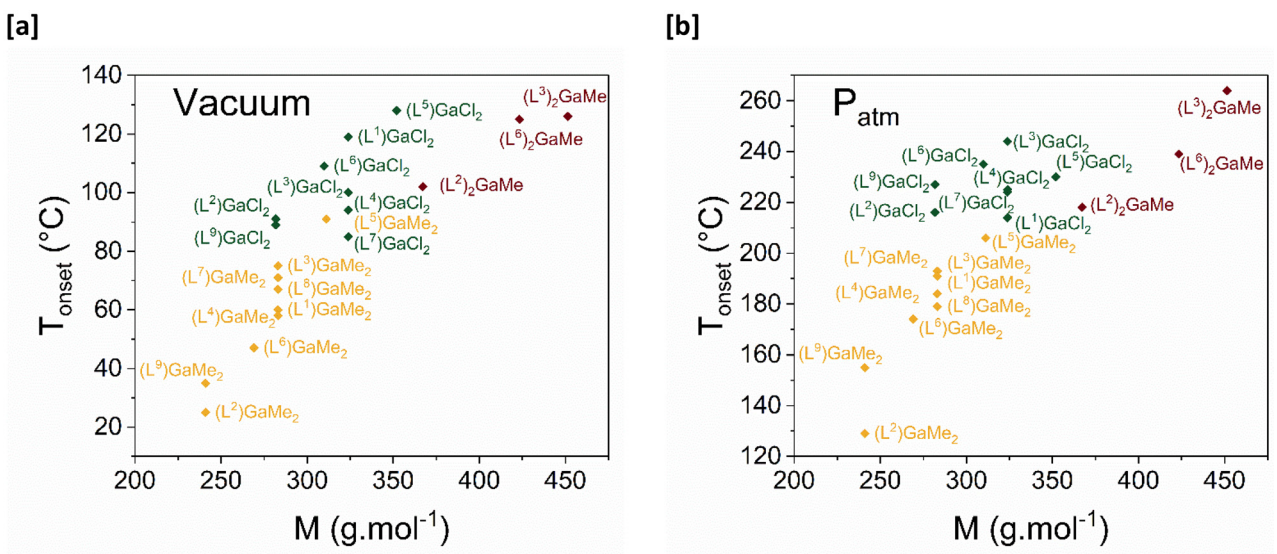

Fig. 2 Influence of the molecular weight on the T_{onset}. Values, extracted from ATG/DSC analyses under [a] reduced pressure and at [b] atmospheric pressure.

tuent on the endocyclic carbon (^{t}Bu, ^{n}Bu, and ^{s}Bu). According to reduced-pressure TG/DSC, **(L^1)GaCl$_2$** is the only complex displaying a sublimation endothermic peak (T_s = 137 °C), while the others exhibit a melting peak followed by a vaporization peak. Among their methylated counterparts, **(L^4)GaMe$_2$** appears to be the most volatile, whereas **(L^1)GaMe$_2$** shows the fastest vaporization rate. For this series of six complexes, the presence of a bulky ^{t}Bu group on the endocyclic carbon leads to greater decomposition (see ESI, Fig. S7†). The comparison of **(L^8)** and **(L^7)**-based complexes further evaluates the combined effect of endocyclic substituent branching and symmetry. While **(L^8)** and **(L^7)**-based complexes show a large difference in onset vaporization temperature, their TG profiles remain similar (see ESI, Fig. S8†). These findings suggest that introducing bulky substituents on the endocyclic carbon in a dissymmetric complex enhances volatility, making these structures particularly relevant for applications requiring volatile precursors.

Finally, our modular synthesis approach enabled access to up to four gallium amidinate complexes for a given ligand. Due to the low volatility of bis-amidinate chlorinated complexes, only the three methylated derivatives were analysed by TG/DSC for the **(L^2)**, **(L^3)** and **(L^6)** amidinate ligands. Interestingly, **(L^2)$_2$GaMe** and **(L^2)GaCl$_2$** exhibit similar vaporization temperatures despite a significant molecular weight difference (ΔM = 85 g mol^{-1}). However, **(L^2)$_2$GaMe** appears to decompose, as indicated by changes in the TG slope between 100 and 125 °C under reduced-pressure TG/DSC. Similar observations can be made with **(L^3)**-based complexes. Notably, bis-amidinate complexes seem to undergo partial modification under reduced pressure, whereas they remain stable at atmospheric pressure (see ESI, Fig. S9†). This highlights the influence of pressure conditions on their thermal behaviour, which should be systematically investigated for ALD/CVD precursor development.

Conclusions

Understanding and predicting the thermal properties of molecular compounds is of paramount importance for their deployment in applications such as atomic layer deposition (ALD), chemical vapor deposition (CVD), catalysis, and advanced materials synthesis. In this study, we investigated a comprehensive series of 24 gallium amidinate complexes featuring diverse structural motifs, including variations in ligand substituents, symmetry, and co-ligands. Detailed structural analysis, supported by single-crystal X-ray diffraction when possible, was combined with rigorous thermal evaluation using thermogravimetric analysis and differential scanning calorimetry, both under atmospheric and reduced pressure conditions.

Our findings highlight the significant influence of ligand architecture, including the nature of substituent chains, the presence of methyl groups, and overall molecular symmetry, on thermal behavior. Both symmetric and dissymmetric complexes yielded compounds with high volatility and stability, underscoring the versatility of the amidinate ligand framework for tailoring thermal properties.

This systematic study not only offers new insights into structure–thermal property relationships but also provides a valuable dataset for refining predictive models, including empirical and AI-based approaches. Such combined experimental and data-driven strategies will be key to accelerating the discovery and rational design of the next-generation molecular precursors.

Author contributions

P.-A. P.: formal analysis, data curation, and investigation. E. P.: formal analysis, data curation, and writing of the original draft. D. C.: data curation. V. A.: data acquisition. N. C.: formal analysis, data curation. S. B.: formal analysis, data curation. V. L.: formal analysis. A. R.: formal analysis. A. A.: formal analysis, funding acquisition, writing of the original draft. N. S.: lead formal analysis, data curation, funding acquisition, writing of the original draft. All authors discussed the results and contributed to the final manuscript.

Data availability

The data supporting this article have been included as part of the ESI.† Crystallographic data has been deposited at the CCDC for **(L^4)GaCl$_2$** under 2444176, for **(L^1)GaCl$_2$** under 2444177, for **(L^3)GaCl$_2$** under 2444178, for **(L^5)GaCl$_2$** under 2444179, for **(L^2)$_2$GaCl** under 2444180, for **(L^2)GaCl$_2$** under 2444181, for **(L^6)$_2$GaCl** under 2444182, for **(L^1)$_2$GaCl** under 2444183, for **(L^5)GaMe$_2$** under 2444184, and for **(L^2)$_2$GaMe** under 2444185.†

Conflicts of interest

There are no conflicts to declare.

Acknowledgements

This work was supported by the French Agence Nationale de la Recherche under the contract number HANAMI ANR-17-CE09-0022 for P.-A. P. This work has been partly carried out at the Energy4Climate Interdisciplinary Center (E4C) of IP Paris and Ecole des Ponts ParisTech, which is in part supported by 3rd Programme d'Investissements d'Avenir [ANR-18-EUR-0006-02], and by the Foundation of Ecole polytechnique (Chaire "Défis Technologiques pour une Énergie Responsable" financed by TotalEnergies) for E. P. The authors thank Marie-Hélène Chavanne (IRCP) for assistance in sample handling, and CNRS and Ecole polytechnique for financial support.

References

1 S. E. Koponen, P. G. Gordon and S. T. Barry, *Polyhedron*, 2016, **108**, 59–66.

2 H. Zhang, W. Xu, J. Liu, M. Li and B. Yang, *J. Mol. Liq.*, 2019, **282**, 474–483.
3 G. Fayet, P. Rotureau, L. Joubert and C. Adamo, *J. Mol. Model.*, 2010, **16**, 805–812.
4 M. I. Kumskov, S. E. Peshkova, L. A. Ponomareva and K. I. Rezchikova, *Russ. Chem. Bull.*, 1996, **45**, 1840–1843.
5 G. Barra, L. Guadagno, M. Raimondo, M. G. Santonicola, E. Toto and S. Vecchio Ciprioti, *Polymers*, 2023, **15**, 3786.
6 D. E. Clark, *MRS Bull.*, 1993, **18**, 25–31.
7 C. Heider, A. Winter, V. Voß, D. Vogt and T. Seidensticker, *ChemCatChem*, 2023, **15**, e202201307.
8 M. Haenel, L. Schanne and E. Woestefeld, *Erdoel Kohle, Erdgas, Petrochem. Brennst.-Chem.*, 1986, **39**, 505–510.
9 M. Roca, H. Liu, B. Messer and A. Warshel, *Biochemistry*, 2007, **46**, 15076–15088.
10 S. R. Vatcha, *Colloids Surf., A*, 1998, **133**, 99–105.
11 R. Philippe, M. Lacroix, L. Dreibine, C. Pham-Huu, D. Edouard, S. Savin, F. Luck and D. Schweich, *Catal. Today*, 2009, **147**, S305–S312.
12 M. W. Small, S. I. Sanchez, N. S. Marinkovic, A. I. Frenkel and R. G. Nuzzo, *ACS Nano*, 2012, **6**, 5583–5595.
13 M. T. Burchill and P. Leste-Lasserre, *J. Vinyl Addit. Technol.*, 1995, **1**, 250–254.
14 A. Leszczynska, J. Njuguna, K. Pielichowski and J. R. Banerjee, *Thermochim. Acta*, 2007, **2**, 75–96.
15 A. R. R. P. Almeida, B. D. A. Pinheiro, G. P. León, B. Postolnyi, J. P. Araújo and M. J. S. Monte, *Molecules*, 2025, **30**, 1551.
16 H. A. Stecher, A. Sen and A. L. Rheingold, *Inorg. Chem.*, 1989, **28**, 3280–3282.
17 A. Devi, *Coord. Chem. Rev.*, 2013, **257**, 3332–3384.
18 W. A. Herrmann, N. W. Huber and O. Runte, *Angew. Chem., Int. Ed. Engl.*, 1995, **34**, 2187–2206.
19 T. Hatanpää, M. Ritala and M. Leskelä, *Coord. Chem. Rev.*, 2013, **257**, 3297–3322.
20 K.-H. Park and W. J. Marshall, *J. Am. Chem. Soc.*, 2005, **127**, 9330–9331.
21 D. Bijou, T. Cornier, S. Mishra, L. Merzoud, H. Chermette, E. Jeanneau, W. Maudez, G. Benvenuti and S. Daniele, *Eur. J. Inorg. Chem.*, 2021, **2021**, 1976–1983.
22 A. Verchère, S. Mishra, E. Jeanneau, H. Guillon, J.-M. Decams and S. Daniele, *Inorg. Chem.*, 2020, **59**, 7167–7180.
23 R. Gómez-Bombarelli, J. N. Wei, D. Duvenaud, J. M. Hernández-Lobato, B. Sánchez-Lengeling, D. Sheberla, J. Aguilera-Iparraguirre, T. D. Hirzel, R. P. Adams and A. Aspuru-Guzik, *ACS Cent. Sci.*, 2018, **4**, 268–276.
24 A. C. Mater and M. L. Coote, *J. Chem. Inf. Model.*, 2019, **59**, 2545–2559.
25 J. Ferraz-Caetano, F. Teixeira and M. N. D. S. Cordeiro, *Chemosphere*, 2024, **359**, 142257.
26 L. Mage, N. Baati, A. Nanchen, F. Stoessel and T. Meyer, *Process Saf. Environ. Prot.*, 2017, **110**, 43–52.
27 J. C. Dearden, *Environ. Toxicol. Chem.*, 2003, **22**, 1696–1709.
28 A. R. Katritzky, M. Kuanar, S. Slavov, C. D. Hall, M. Karelson, I. Kahn and D. A. Dobchev, *Chem. Rev.*, 2010, **110**, 5714–5789.
29 X. Yan, T. Lan, Q. Jia, F. Yan and Q. Wang, *Fluid Phase Equilib.*, 2020, **507**, 112437.
30 M. Moharramnejad, L. Tayebi, A. R. Akbarzadeh and A. Maleki, *Microporous Mesoporous Mater.*, 2022, **336**, 111815.
31 H. Matsukawa, M. Kitahara and K. Otake, *Fluid Phase Equilib.*, 2021, **548**, 113179.
32 B. Du, Z. Zhang, S. Grubner, J. T. Yurkovich, B. O. Palsson and D. C. Zielinski, *Biophys. J.*, 2018, **114**, 2691–2702.
33 L. Constantinou and R. Gani, *AIChE J.*, 1994, **40**, 1697–1710.
34 V. Van Speybroeck, R. Gani and R. J. Meier, *Chem. Soc. Rev.*, 2010, **39**, 1764.
35 A. Odinokov, W.-J. Son, A. Yakubovich, J. Y. Park and Y. Jung, *J. Chem. Theory Comput.*, 2024, **20**, 6144–6151.
36 S. T. Barry, *Coord. Chem. Rev.*, 2013, **257**, 3192–3201.
37 P. Kaur, L. Mai, A. Muriqi, D. Zanders, R. Ghiyasi, M. Safdar, N. Boysen, M. Winter, M. Nolan, M. Karppinen and A. Devi, *Chem. – Eur. J.*, 2021, **27**, 4913–4926.
38 R. G. Gordon, B. S. Lim, US7557229B2, 2009.
39 S. B. Kim, C. Yang, T. Powers, L. M. Davis, X. Lou and R. G. Gordon, *Angew. Chem., Int. Ed.*, 2016, **55**, 10228–10233.
40 M. Eleter, S. Daniele, V. Brize, C. Dubourdieu, C. Lachaud, N. Blasco and A. Pinchart, *ECS Trans.*, 2009, **25**, 151.
41 P. J. Pallister, S. C. Buttera and S. T. Barry, *J. Phys. Chem. C*, 2014, **118**, 1618–1627.
42 P. J. Pallister, S. C. Buttera and S. T. Barry, *Phys. Status Solidi A*, 2015, **212**, 1514–1518.
43 S. Dagorne, R. F. Jordan and V. G. Young, *Organometallics*, 1999, **18**, 4619–4623.
44 M. P. Coles, D. C. Swenson, R. F. Jordan and V. G. Young, *Organometallics*, 1997, **16**, 5183–5194.
45 S. Dagorne, I. A. Guzei, M. P. Coles and R. F. Jordan, *J. Am. Chem. Soc.*, 2000, **122**, 274–289.
46 A. Willner, A. Hepp and N. W. Mitzel, *Dalton Trans.*, 2008, 6832.
47 C. Holzhacker, M. J. Calhorda, A. Gil, M. D. Carvalho, L. P. Ferreira, B. Stöger, K. Mereiter, M. Weil, D. Müller, P. Weinberger, E. Pittenauer, G. Allmaier and K. Kirchner, *Dalton Trans.*, 2014, **43**, 11152–11164.
48 C. Holzhacker, C. M. Standfest-Hauser, M. Puchberger, K. Mereiter, L. F. Veiros, M. J. Calhorda, M. D. Carvalho, L. P. Ferreira, M. Godinho, F. Hartl and K. Kirchner, *Organometallics*, 2011, **30**, 6587–6601.
49 P. Schiltz, N. Casaretto, S. Bourcier, A. Auffrant and C. Gosmini, *Dalton Trans.*, 2023, **52**, 14859–14866.
50 A. Hock, M. J. Foody, US20230167548A1, 2023.
51 C. Jones, S. Aldridge, T. Gans-Eichler and A. Stasch, *Dalton Trans.*, 2006, 5357.
52 A. L. Brazeau, G. A. DiLabio, K. A. Kreisel, W. Monillas, G. P. A. Yap and S. T. Barry, *Dalton Trans.*, 2007, 3297.

53 A. W. Addison, T. N. Rao, J. Reedijk, J. Van Rijn and G. C. Verschoor, *J. Chem. Soc., Dalton Trans.*, 1984, 1349–1356.
54 A. G. Blackman, E. B. Schenk, R. E. Jelley, E. H. Krenske and L. R. Gahan, *Dalton Trans.*, 2020, **49**, 14798–14806.
55 E. Pugliese, D. Coutancier, P.-A. Pavard, J. Hervochon, B. Van Der Linden, N. Casaretto, S. Bourcier, G. Pourtois, M. Bouttemy, A. Auffrant and N. Schneider, *Dalton Trans.*, 2025, **54**, 5182–5191.
56 R. Král, P. Zemenová, V. Vaněček, A. Bystřický, M. Kohoutková, V. Jarý, S. Kodama, S. Kurosawa, Y. Yokota, A. Yoshikawa and M. Nikl, *J. Therm. Anal. Calorim.*, 2020, **141**, 1101–1107.